THE JOURNAL OF PHYSICAL CHEMISTRY B

Article

pubs.acs.org/JPCB

Out-of-Plane Low-Frequency Vibrations and Nonradiative Decay in the $^1\pi\pi^*$ State of Jet-Cooled 5-Methylcytosine

Maria A. Trachsel, Simon Lobsiger, and Samuel Leutwyler*

Department of Chemistry and Biochemistry, University of Bern, Freiestrasse 3, CH-3012 Bern, Switzerland

Supporting Information

ABSTRACT: We investigate the UV vibronic spectrum and excited-state nonradiative processes of jet-cooled 5-methylcytosine (5MCyt) using two-color resonant two-photon ionization spectroscopy at 0.3 and 0.05 cm^{-1} resolution. In contrast to cytosine, which shows only five bands above its electronic origin, the lowest electronic transition of 5MCyt exhibits about 25 low-frequency vibronic bands that extend to 0_0^0 + 450 cm^{-1}, allowing to extract detailed information on the excited-state electronic and nuclear structure. Most bands are overtones and combinations of the out-of-plane vibrations ν'_1, ν'_2, and ν'_3. Their large intensities reflect butterfly-, boat-, and twist-deformations of the 5MCyt framework upon electronic excitation. From the rotational contours of the 0_0^0, 1_0^2, 2_0^2, and 3_0^2 bands, the transition is found to be polarized along the in-plane a/b axes, characteristic of a $^1\pi\pi^*$ transition. Approximate second-order coupled-cluster (CC2) and time-dependent B3LYP calculations both predict that 5MCyt undergoes an out-of-plane deformation in its $^1\pi\pi^*$ (S_2) state but both methods overestimate the out-of-plane ν'_1, ν'_2, and ν'_3 vibrational frequencies by a factor of 3−5. The TD-B3LYP $^1\pi\pi^*$ transition dipole moment direction is 10%:90% a:b, in good agreement with experiment. From the Lorentzian line shape contributions needed to fit the rotational contours, a lower limit to the 5MCyt $^1\pi\pi^*$ state lifetime at the 0_0^0, 1_0^2, 2_0^2, and 3_0^2 bands is determined as $\tau \geq 30$ ps. These values are in stark contrast to the ultrafast (picosecond) lifetimes measured for jet-cooled cytosine by femtosecond pump−probe techniques. They also confirm the observation from the R2PI spectrum that 5-methylation of cytosine increases its excited-state lifetime. The higher out-of-plane overtone and combination bands disappear from the spectrum by ∼460 cm^{-1}, signaling the onset of lifetimes $\tau < 0.5$ ps, induced by excitation of the ν'_1, ν'_2, and ν'_3 modes. Above 460 cm^{-1} the in-plane fundamentals 9_0^1, 10_0^1, and 17_0^1 are weakly observed, implying that the in-plane vibrations couple weakly to the out-of-plane modes and have lifetimes $\tau > 3$ ps up to 720 cm^{-1} excess vibrational energy.

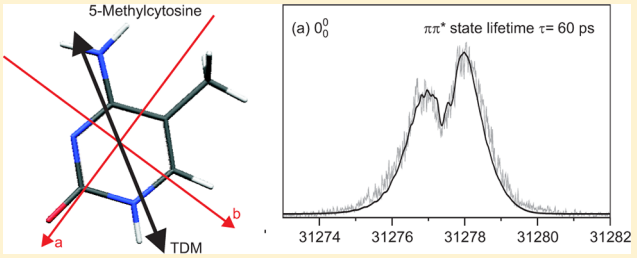

I. INTRODUCTION

DNA methylation is widespread in plants, fungi, and animals[1] and is an important epigenetic mark for regulating chromatin structures and gene expression.[2−4] In higher eukaryotes, methylation of DNA occurs at the C_5 position of cytosine,[2] which is catalyzed by a family of conserved methyltransferases.[1] The modification occurs largely in the CG dinucleotide of various double-stranded sequences.[2] There is clear evidence that DNA methylation switches off eukaryotic gene expression, particularly when it occurs in the promoter regions upstream of the gene's transcribed sequences. The methyl group of 5-methylcytosine projects into the DNA major groove, where it interacts with DNA-binding proteins without perturbing the double helical structure of the DNA. In plants, about 30% of all cytosine is methylated, whereas in vertebrates the fraction is lower (3−6%), demonstrating the biological importance of methylcytosines.

Cytosine is believed to be one of the molecules formed on early Earth that survived photolysis by the intense UV solar radiation due to highly efficient and nonreactive radiationless relaxation from its excited states, implying a photochemical selection of the molecular building blocks of life.[5−7] In this context it is important to investigate and compare the lowest optical transitions and vibronic lifetimes of cytosine and its methylated derivatives. These show which vibrations couple to the electronic transitions, at which excess vibrational energy the coupling to the ground or other excited states commences, and reveal the promoting modes for the radiationless deactivation.

De Vries et al. have performed pioneering resonant two-photon ionization (R2PI) UV and mid-IR spectra of jet-cooled cytosine and 5-methylcytosine.[8−10] They observed an electronic origin of 5MCyt at 31 269 cm^{-1}, followed by a few vibronic bands to higher energy, which they assigned to the amino-keto N1H (**1**) tautomer; see Figure 1.[8,9] They assigned a higher-energy part of the R2PI spectrum that appears around 36 000 cm^{-1} to the amino-enol tautomer.[8,9] However, the bands were not vibrationally assigned nor was experimental evidence given for the assignment as a $^1\pi\pi^*$ transition. This is especially relevant, since 5MCyt is calculated to have a $^1n_O\pi^*$ state that lies closely beneath the $^1\pi\pi^*$ state, see below.

Received: June 11, 2012
Revised: August 15, 2012
Published: August 15, 2012

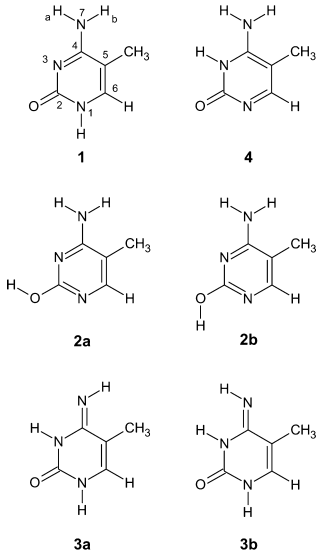

Figure 1. Six most stable tautomeric forms of gas-phase 5-methylcytosine. The numbers follow those given in ref 25. The calculated relative energies of the different tautomers are compiled in Table 1.

Lapinski et al.[11] have investigated the infrared (IR) spectra of 5MCyt in low-temperature Ar matrices. They observed the spectra of three species, which they assigned to the amino-keto (**1**), amino-enol (**2**), and imino-keto (**3**) tautomers (as numbered in Figure 1).[11] Based on these tautomer assignments, they were able to assign most of the IR bands.[11] Feyer et al.[12] investigated core-level X-ray photoemission and near-edge X-ray absorption fine structure spectra of 5MCyt. They found the same three tautomeric forms as Lapinski et al.[11]

In this work, we analyze the low-energy vibronic bands in the two-color resonant two-photon ionization (2C-R2PI) spectrum of 5MCyt in detail. We show that the 12 lowest bands can be systematically assigned to overtones and combinations of the three lowest out-of-plane framework vibrations of the amino-keto (**1**) tautomer. The rotational contours of the lowest four vibronic bands in the R2PI spectrum are measured and analyzed, giving the orientation of the respective electronic and vibronic transition-dipole moments in the 5-methylcytosine molecular frame. The measurements are accompanied by CC2 and TD-B3LYP calculations of the lowest excited singlet and triplet states. A group of weak bands is observed 150 cm^{-1} below the electronic origin of 5MCyt; these are assigned as hot bands of the same $^1\pi\pi^*$ transition.

II. COMPUTATIONAL METHODS AND RESULTS

A. Computational Methods. The electronic ground state of all 14 tautomers and rotamers of 5-methylcytosine were first optimized using density functional theory (B3LYP), with the TZVP basis set. The ground state structures of the six most stable tautomers were then reoptimized at the correlated level, using the Møller-Plesset (MP2) method in the resolution-of-identity (RI) approximation and the aug-cc-pVXZ (X = D,T) basis sets, and also with the spin-component scaled (SCS) MP2 method and the aug-cc-pVTZ basis set. Both ground- and excited-state calculations were performed with the second-order approximate coupled-cluster (CC2) method in the RI approximation, using the aug-cc-pVXZ (X = D,T) basis sets. Excited state calculations were also performed using the time-dependent B3LYP DFT method with the TZVP basis set. Vertical and adiabatic excitation energies were calculated with the B3LYP and CC2 methods to the S_n and T_n (n = 1,2,3) states.

Normal-mode calculations were performed for all geometry-optimized structures to ensure that they correspond to true minima on the potential energy surface. The following thresholds were decreased to nonstandard values: The thresholds for SCF and one-electron density convergence were set to 10^{-9} and 10^{-8} a.u., respectively. The convergence thresholds for all structure optimizations were set to 10^{-8} a.u. for the energy change, 6×10^{-6} a.u. for the maximum displacement element, 10^{-6} a.u. for the maximum gradient element, 4×10^{-6} a.u. for the rms displacement, and 10^{-6} a.u. for the rms gradient. The calculations were performed using Turbomole 6.0.[13]

B. Tautomer Energies. Figure 1 shows the schematic structures of the six most stable tautomers of 5MCyt. In Table 1 we report the relative energies of the different 5MCyt tautomers and rotamers calculated at the density-functional (B3LYP) and at the MP2, CC2, and SCS-MP2 correlated levels of theory. The MP2, CC2, and SCS-MP2 methods with the aug-cc-pVTZ basis set all predict the amino-enol-trans (**2b**) as the most stable tautomer. The high-level CCSD/cc-pVTZ

Table 1. Relative Energies of 5-Methylcytosine Tautomers and Rotamers at Different Levels of Theory (in kcal/mol)

	B3LYP TZVP	B3LYP 6-31+G(d,p)[a]	MP2 aug-cc-pVTZ	CC2 aug-cc-pVTZ	SCS-MP2 aug-cc-pVTZ	CCSD cc-pVTZ[b]
amino-keto N1H (**1**)	0.00	0.06	2.30	0.62	1.08	1.74
amino-enol-trans (**2b**)	0.79	0.00	0.00	0.00	0.00	0.00
amino-enol-cis (**2a**)	1.59	0.83	0.73	0.73	0.73	0.72
imino-keto-cis (**3b**)	1.86	2.36	4.27	3.20	1.81	1.87
imino-keto-trans (**3a**)	0.63	1.16	2.91	1.89	0.55	0.70
amino-keto N3H (**4**)	7.42	7.41	10.04	8.07	9.02	
imino-enol-cis−trans N1H	26.75	26.41				
imino-enol-cis−cis N1H	17.09	16.79				
imino-enol-trans−trans N1H	32.16	31.96				
imino-enol-trans−cis N1H	21.58	21.35				
imino-enol-cis−trans N3H	15.34	15.08				
imino-enol-cis−cis N3H	24.67	24.40				
imino-enol-trans−trans N3H	12.86	12.56				
imino-enol-trans−cis N3H	21.10	20.80				

[a]Tian et al.[14] [b]Feyer et al.[12]

dx.doi.org/10.1021/jp305688m | J. Phys. Chem. B 2012, 116, 11081−11091

calculations of Feyer et al.[12] predict the same energetic order as the SCS-MP2/aug-cc-pVTZ method, **2b** < **3a** < **2a** < **1** < **3b** < **4**, and the CCSD and SCS-MP2 calculations also predict similar relative tautomer energies, as can be seen in Table 1. From this good agreement of the SCS-MP2 method with the high-level results of Feyer et al.,[12] we consider the SCS-MP2 energies to be reliable. In contrast to the correlated calculations, the B3LYP density functional places the amino-keto N1H tautomer **1** below the amino-enol-trans form **2b**.

The relative energies of the imino-enol tautomers and rotamers have been previously calculated by Tian et al. at the B3LYP/6-31G+(d,p) level;[14] we confirm their values at the B3LYP/TZVP level. Table 1 shows that all imino-enol forms lie >13 kcal/mol above the most stable tautomer **2b**, hence we do not consider them any further.

C. Excited States and Excited-State Vibrations. Table 2 summarizes the adiabatic transition energies of the six 5MCyt tautomers shown in Figure 1, calculated with the CC2 and TD-B3LYP methods. As can be seen, only the transitions of the amino-keto tautomers **1** and **4** lie in the 31 000−32 000 cm^{-1} region covered in this work, while those of the amino-enol and imino-keto tautomers are shifted by ~6000 cm^{-1} to the blue. The lowest $^1\pi\pi^*$ ($S_2 \rightarrow S_0$) transition of the **4** (N3H) tautomer is predicted to lie very close to that of the **1** (N1H) tautomer. However, tautomer **4** is calculated to be 7−10 kcal/mol less stable than tautomer **1**, see Table 1; hence, we do not expect this tautomer in the supersonic jet.

Table 2. CC2/aug-cc-pVDZ and TD-B3LYP/TZVP Calculated Adiabatic Energies of the S_1, S_2, and T_1 States of the Low-Lying Tautomers and Rotamers of 5-Methylcytosine (in eV)

tautomer	transition	CC2	B3LYP	expt
amino-keto N1H (**1**)	$^1n_O\pi^*$	3.17	3.72	
	$^1\pi\pi^*$	3.64	3.90	3.88
	$^3\pi\pi^*$		3.01	
amino-enol-trans (**2b**)	$^1n_O\pi^*$	4.49[a]	4.41	
	$^1\pi\pi^*$	4.35	4.82[a]	
	$^3\pi\pi^*$		3.72	
amino-enol-cis (**2a**)	$^1n_O\pi^*$	5.04[a]	4.30	
	$^1\pi\pi^*$	4.24	4.81[a]	
	$^3\pi\pi^*$		3.52	
imino-keto-cis (**3b**)	$^1n_O\pi^*$	2.91	3.07	
	$^1\pi\pi^*$	5.00	4.65[a]	
	$^3\pi\pi^*$		2.75	
imino-keto-trans (**3a**)	$^1n_O\pi^*$	2.96	3.12	
	$^1\pi\pi^*$	5.04	6.81[a]	
	$^3\pi\pi^*$		2.77	
amino-keto N3H (**4**)	$^1n_O\pi^*$	2.97	3.66	
	$^1\pi\pi^*$	3.62[a]	3.90	
	$^3\pi\pi^*$		2.88	

[a]In C_s symmetry.

In the B3LYP/TZVP S_0 optimized structure, the 5-methylpyrimidinone framework is C_s symmetric, but the amino group is slightly pyramidal. The pyramidalization of the amino group is more pronounced in the CC2/aug-cc-pVDZ ground state. The B3LYP and CC2 predicted geometry changes upon $^1\pi\pi^*$ excitation are (i) an increase in the pyramidalization of the amino group, (ii) a twist around the $C^5{=}C^6$ double bond (the $C^4C^5C^6H$ dihedral angle increases by +4.1° and the $N^3C^4C^5C^8$ dihedral decreases by −1.1°), (iii) in-plane deformation of the pyrimidinone, with contractions of the $N^1{-}C^2$, $C^2{-}N^3$, and $C^4{-}C^5$ bonds and expansions of the $C^2{=}O$, $N^3{=}C^4$, $C^5{=}C^6$, and $C^6{-}N^1$ bonds. The $C^4C^5C^8$ and C^5C^6H angles change by −1.7° and 2.7°, respectively. Figure 2 shows the CC2/aug-cc-pVDZ calculated geometries and geometry changes of 5MCyt. The CC2/aug-cc-pVDZ and B3LYP/TZVP ground and $^1\pi\pi^*$ state geometry parameters, bond length and angle changes upon $^1\pi\pi^*$ excitation are given in the Supporting Information.

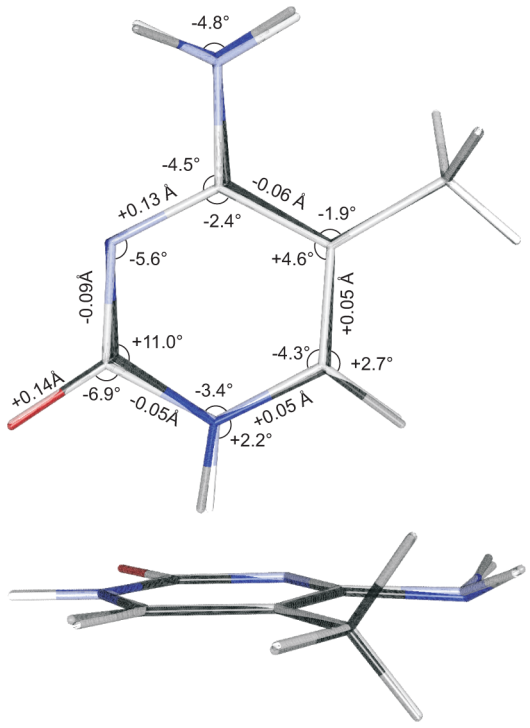

Figure 2. CC2/aug-cc-pVDZ calculated geometries and geometry changes of 5-methylcytosine upon $^1\pi\pi^*$ excitation (ground state in light color). Bond length changes ≥0.05 Å and bond angle changes ≥1° are indicated.

Table 3 compares the calculated adiabatic and vertical transition energies for the amino-keto N1H (**1**) tautomer. In both the B3LYP/TZVP and CC2/aug-cc-pVTZ calculations, the $^1n_O\pi^*$ state is 0.20−0.29 eV above the $^1\pi\pi^*$ state when considering vertical energies but drops 0.18−0.48 eV below the

Table 3. CC2/aug-cc-pVDZ and TD-B3LYP/TZVP Calculated Adiabatic and Vertical Transition Energies and Electronic Oscillator Strengths *f* for the Amino-Keto N1H (1) Tautomer

	CC2			B3LYP			exp	
state (transition)	vert./ eV	adiab./ eV	f^a	vert./ eV	adiab./ eV	f^a	eV	
$^1n_O\pi^*$	4.77	3.23	0.002	4.79	3.72	0.001		
$^1\pi\pi^*$	4.48	3.71	0.053	4.59	3.90	0.044	3.88	
$^3\pi\pi^*$	3.69			3.33	3.01			
$^3\pi\pi^*$	4.64			4.15				
$^3n\pi^*$	4.71			4.50				

[a]Vertical excitation from S_0 equilibrium geometry, length representation.

dx.doi.org/10.1021/jp305688m | J. Phys. Chem. B 2012, 116, 11081−11091

$^1\pi\pi^*$ state for adiabatic transitions. The $^1n_O\pi^*$ excitation is predicted to be 30−50 times weaker than the $^1\pi\pi^*$ excitation; therefore, optical excitation should occur primarily to the $^1\pi\pi^*$ state. The adiabatic and vertical transition energies of the other tautomers and rotamers are given in the Supporting Information.

The CC2/aug-cc-pVDZ calculated molecular orbitals that are involved in the $^1n_O\pi^*$ and $^1\pi\pi^*$ transitions are shown in Figure 3. Upon $\pi\pi^*$ excitation, electron density moves from the C═O

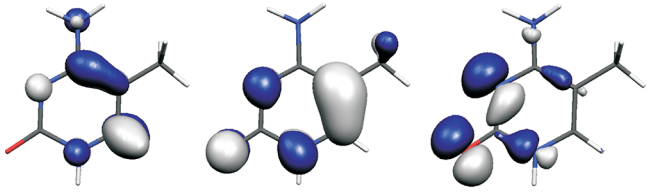

Figure 3. HOMO-1 *n*, HOMO π, and LUMO π^* orbitals of 5-methylcytosine (CC2/aug-cc-pVDZ).

oxygen into the pyrimidine ring; this lowering of the π bond order leads to a lengthening of the C═O bond distance, as reflected in the calculations (B3LYP, +0.11 Å,; CC2, +0.14 Å). The HOMO → LUMO excitation changes the C^5═C^6 double bond from π-bonding to π-antibonding, which renders the framework susceptible to twisting around C^5═C^6. The C^4−C^5 single bond gains π-bonding character and some π-electron density moves onto the amino N atom.

Table 4 gives the B3LYP and CC2 calculated harmonic $^1\pi\pi^*$ state vibrations and frequencies for the amino-keto N1H (**1**) tautomer of 5MCyt. The description is based on the TD-B3LYP/TZVP eigenvectors. The designation of the ring distortion follows the Wilson nomenclature for benzene derivatives.[15] The lowest three nine modes are out-of-plane deformation vibrations. The first in-plane vibration is the ν'_4 mode at 282 cm^{-1}. The Supporting Information gives an analogous Table of the calculated $^1\pi\pi^*$ vibrations with mode descriptions for the CC2/aug-cc-pVDZ calculation. Compared to the TD-B3LYP calculation, the CC2 calculation predicts that ν_4 and ν_6 are out-of-plane modes, resulting in nine out-of-plane vibrations below 470 cm^{-1}.

III. EXPERIMENTAL METHODS AND RESULTS

A. Methods. The experimental setup for two-color R2PI measurements has been previously described.[16,17] Neon carrier gas (Linde, ≥99.995%) at ∼1.8 bar backing pressure was passed through a 20 Hz pulsed nozzle (0.4 mm diameter) containing 5MCyt (Alfa Aesar, 97%) that was heated to 225 °C. Two-color resonant two-photon ionization (2C-R2PI) spectra were measured by crossing the skimmed supersonic jet with the unfocused UV excitation and ionization laser beams in the source of a linear time-of-flight mass spectrometer (TOF-MS). Excitation was performed with 400−600 μJ UV pulses from a frequency-doubled Radiant Dyes NarrowScan DR dye laser. For rotational contour measurements the energy of the excitation laser was reduced to ∼250 μJ/pulse. The bandwidth in the visible is ∼0.037 cm^{-1}, as measured with a HighFinesse Ångstrom WS6 high precision wavemeter. After frequency doubling, the bandwidth in the UV is expected to be $\sqrt{2}$ wider (0.05 cm^{-1} or 1555 MHz). The spectra were recorded at 0.012 cm^{-1} step size. The frequency scale is calibrated by measuring the fundamental frequency with the WS6 wavemeter. Ionization light pulses of ∼100 μJ at 226 nm were produced by an Ekspla

Table 4. Calculated Harmonic $^1\pi\pi^*$ State Vibrations and Frequencies (in cm^{-1}) for the Amino-Keto N1H (1) Tautomer of 5-Methylcytosine at the CC2 and B3LYP Levels

mode	irrep.[a]	description[b]	CC2/ aVDZ	B3LYP/ TZVP	exp.[c]
ω_1	a″	CH_3 torsion	98.1	57.0	
ν_1	a″	ring twisting/γCH_3/γC_2O	120.2	131.6	(24.2)
ν_2	a″	butterfly	158.2	159.3	(34.6)
ν_3	a″	$\gamma C_6H/\gamma C_6/\gamma N_1H$	212.7	200.6	(84.4)
ν_4	a′	$\beta_{as}NH_2/\delta CH_3$	259.9	281.5	
ν_5	a″	$\gamma_{as}NH_2/\gamma C_6H/\gamma C_5$	285.1	328.0	
ν_6	a′	$\beta_{as}NH_2/\delta C_2O/\delta CH_3$	325.8	345.0	
ν_7	a″	$\gamma C_6H/\gamma_{as}NH_2$	329.2	390.8	
ν_8	a″	$\gamma_{as}NH_2/\gamma C_6H$	368.2	414.8	
ν_9	a′	6b	469.6	488.6	468
ν_{10}	a′	6a	483.6	526.9	514
ν_{11}	a″	γN_1H	505.1	540.0	
ν_{12}	a′	3	539.9	578.2	
ν_{13}	a″	$\gamma C_4/\gamma C_5/\gamma N_1H$	547.7	612.1	
ν_{14}	a″	NH_2 inversion	646.3	467.9	
ν_{15}	a″	$\gamma N_1H/\gamma C_2$	675.7	746.4	
ν_{16}	a′	$\delta N_1C_6C_5/\delta C_2N_3C_4/\nu C_2O$	719.4	777.0	
ν_{17}	a′	$1/\nu C_2O$	739.7	761.6	731.2
ν_{18}	a′	$\nu N_3C_4/\delta N_1H/\delta C_6H/\beta_{as}NH_2/\beta_{as}CH_3$	885.7	957.7	
ν_{19}	a′	$\delta C_2/\beta_{as}NH_2/\delta N_1H$	962.7	1137.5	
ν_{20}	a′	$\beta_{as}CH_3/\beta_{as}NH_2$	993.1	985.5	
ν_{21}	a″	CH_3 deformation antisymm.	1027.5	1045.4	
ν_{22}	a′	$\delta N_1C_2N_3/\beta_{as}NH_2/\delta N_1H$	1045.7	1070.4	
ν_{23}	a′	$\nu N_1C_6/\nu C_2O/\beta_{as}NH_2/\delta N_1H/\delta C_6H$	1143.5	1202.9	
ν_{24}	a′	$\beta_{as}NH_2/\nu C_5CH_3$	1202.7	1212.2	
ν_{25}	a′	δC_6H	1239.9	1282.7	
ν_{26}	a′	$15/\delta N_7H_b$	1303.4	1338.3	
ν_{27}	a′	CH_3 umbrella/δN_1H	1377.6	1412.9	
ν_{28}	a′	CH_3 umbrella/$\nu C_4NH_2/\delta N_1H$	1396.6	1434.0	
ν_{29}	a′	$\beta_sCH_3/\delta N_1H/\delta C_6H/\nu C_5C_6$	1450.6	1517.6	
ν_{30}	a″	CH_3 deformation antisymm.	1466.0	1484.6	
ν_{31}	a′	$\beta_sCH_3/\delta N_1H/\delta C_6H$	1490.3	1496.4	
ν_{32}	a′	$\nu C_2N_3/\nu C_4C_5/\delta C_6H/\delta N_1H$	1582.3	1545.2	
ν_{33}	a′	β_sNH_2	1594.1	1645.6	
ν_{34}	a′	$\beta_sNH_2/\nu C_4C_5/\nu C_2N_3$	1626.0	1620.4	
ν_{35}	a′	ν_sCH_3	3033.5	3009.3	
ν_{36}	a″	$\nu_{as}CH_3$	3107.3	3051.0	
ν_{37}	a′	$\nu_{as}CH_3$	3149.4	3107.9	
ν_{38}	a′	νC_6H	3254.5	3273.4	
ν_{39}	a′	ν_sNH_2	3501.0	3567.1	
ν_{40}	a′	νN_1H	3588.4	3636.1	
ν_{41}	a′	$\nu_{as}NH_2$	3628.7	3688.9	

[a]Irreducible representation in the C_s point group. [b]Description based on B3LYP/TZVP calculation; ν = stretching vibration; δ = in-plane deformation vibration; γ = out-of-plane deformation vibration; β_s = scissoring vibration; β_{as} = in-plane rocking vibration; γ_s = out-of-plane wagging vibration; γ_{as} = torsion vibration. [c]Observed vibronic fundamentals corresponding to in-plane vibrations and out-of-plane fundamentals (in parentheses) are estimated as half the overtone frequency.

dx.doi.org/10.1021/jp305688m | J. Phys. Chem. B 2012, 116, 11081−11091

NT342B optical parametric oscillator (UV-OPO, 4−6 cm^{-1} bandwidth).

A frequency-doubled Lambda-Physik FL3002 dye laser giving ~350 μJ pulses in the UV was used as the depletion laser for UV/UV hole-burning experiments. Excitation and ionization was performed as for the R2PI experiments. The depletion laser was fired 600 ns before the excitation and ionization laser pulses.

B. Two-Color Resonant Two-Photon Ionization and UV/UV Hole Burning Spectra. Figure 4 shows the

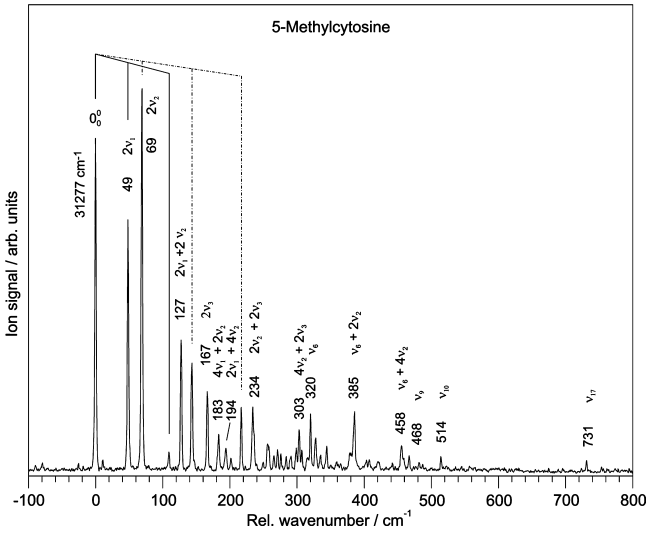

Figure 4. $\pi\pi^*$ ← S_0 two-color resonant two-photon ionization spectrum of supersonically cooled 5-methylcytosine (ionization at 226 nm). The frequency scale is relative to the electronic origin at 31 277.4 cm^{-1}.

vibrationally resolved two-color resonant two-photon ionization spectrum of supersonically 5MCyt over a range of 31 000−32 000 cm^{-1} when ionizing at 226 nm. The spectrum exhibits a sharp 0_0^0 band at 31 277 cm^{-1} (3.878 eV). De Vries et al.[8] have previously identified the origin of 5MCyt at 31 269 cm^{-1}; the difference is due to the vacuum correction for our wavenumber value. The experimental value is in very good agreement with the B3LYP/TZVP predicted S_2 ← S_0 adiabatic transition energy of 31 431 cm^{-1} (3.897 eV). This concurs with previous findings of Marian and co-workers for cytosine.[18] In contrast, the CC2/aug-cc-pVDZ adiabatic transition energy is 0.24 eV (1940 cm^{-1}) too low, see Table 2. The CC2 prediction improves somewhat with the larger aug-cc-pVTZ basis set, see Table 3.

Within the first 250 cm^{-1} above the electronic origin about 12 vibronic excitations with very low frequencies are observed. These are out-of-plane vibrational overtones and combinations that will be analyzed in the next section. Above +250 cm^{-1}, the density of vibronic transitions increases sharply. Above +460 cm^{-1}, the band intensities decrease to nearly zero, with the exception of three weak bands at 468, 514, and 731 cm^{-1}.

Figure 5 compares the 2C-R2PI spectrum of 5MCyt (a) with the UV/UV hole-burning spectrum (b). The hole-burning laser was set to the strongest UV band at 31 347 cm^{-1}, which is assigned as 2_0^2 (see below). All bands up to +400 cm^{-1} also appear in the hole-burning spectrum and therefore belong to the same ground state of the same tautomeric species. Five weak bands to the red of the 0_0^0 band do not appear in the

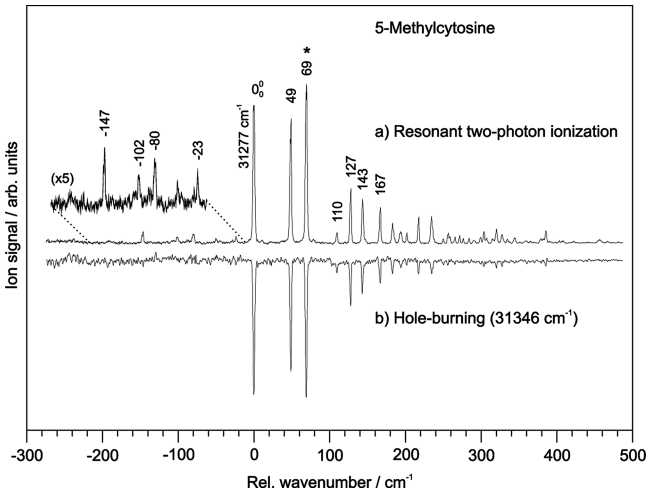

Figure 5. UV/UV hole-burning spectrum of 5-methylcytosine. The UV hole-burning laser was fixed at the most intense band at 31 347 cm^{-1}, marked with an asterisk.

holeburning spectrum. Although the signal/noise level is relatively low in this region, the absence of these bands implies that they do *not* originate from the cold $\nu'' = 0$ ground state level, see also the Discussion.

C. Rotational Band Contours. 5-Methylcytosine is an asymmetric top with its *c* inertial axis perpendicular to and its *a*/*b* axes within the pyrimidinone plane. The in-plane axes are drawn in red in Figure 6. Figure 7 shows the experimental

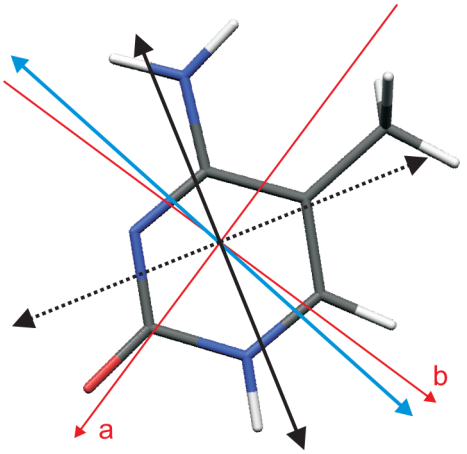

Figure 6. B3LYP/TZVP calculated (blue) and experimental (full and dashed black) transition dipole moment (TDM) vectors for the $^1\pi\pi^*$ transition of 5-methylcytosine. The inertial *a* and *b* axes are in red. There is a sign ambiguity for the experimental TDM. Both possible orientations are given; the preferred orientation is drawn in black.

rotational contours of the 0_0^0 origin and of the 1_0^2, 2_0^2 and 3_0^2 bands, measured at 0.052 cm^{-1} resolution. The band assignments will be discussed in section E. The 0_0^0 contour lacks the strong central peak that would indicate *c*-type polarization, but shows a double-wing *a*/*b*-hybrid shape that is characteristic for an in-plane $\pi\pi^*$ electronic transition. Since the 1_0^2, 2_0^2 and 3_0^2 vibronic bands show the same type of contour, their upper levels must also be totally symmetric (a' in C_s).

The rotational contours were simulated with the program PGOPHER[19] using an asymmetric rigid-rotor Hamiltonian. Table 5 summarizes the CC2 and the B3LYP/TD-B3LYP

dx.doi.org/10.1021/jp305688m | J. Phys. Chem. B 2012, 116, 11081−11091

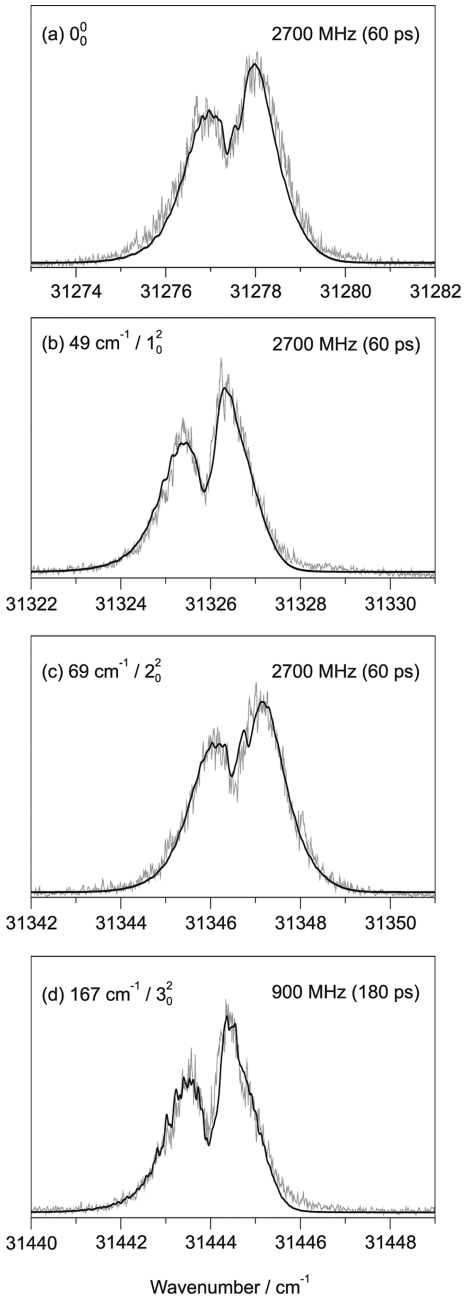

Figure 7. Rotational band contours of the 0_0^0, 1_0^2, 2_0^2, and 3_0^2 out-of-plane overtone bands of supersonically cooled 5-methylcytosine. All experiments are at 0.05 cm^{-1} resolution and with ionization at 226 nm. For (a,b) the fitted asymmetric rotor contour for dominantly in-plane ($\pi\pi^*$) transitions is drawn in black. The contour fit parameters are listed in Table 5.

calculated rotational constants for the S_0 and S_2 ($^1\pi\pi^*$) states. For all contour fits, the B3LYP S_0 state constants A″, B″ and C″ were used as fixed inputs. The TD-B3LYP S_2 values A′, B′, and C′ (see Table 5) were used as initial values for the fits. The fitted B′ and C′ constants were found to differ by less than the fit error (±30 MHz) from the TD-B3LYP values, hence the TD-B3LYP values were retained. Identical rotational constants were used for the 0A′ ← 0A″ and 1E′ ← 1E″ subbands. The A−A/E−E torsional subband splitting, which is calculated to be 0.2 cm^{-1} at the B3LYP/TD-B3LYP level (see section E), had to be increased to 0.3 cm^{-1} for a satisfactory fit, see Table 5.

The laser line shape is assumed to be Gaussian with a fwhm of Δ_{Gauss} = 1555 MHz, see section III. We varied the ground-state rotational temperature T_{rot} between 2 and 8 K and found optimum agreement with experiment for T_{rot} = 4.5 K. This is in good agreement with the T_{rot} = 3−5 K found in previous measurements for other pyrimidines and purines.[16,17,20] The parameter uncertainties given in Table 5 were estimated by varying each parameter independently until the fit changed significantly.

The TD-B3LYP calculated $^1\pi\pi^*$ electronic transition dipole moment (TDM) vector is plotted in blue in Figure 6. The TD-B3LYP TDM components μ_a, μ_b, and μ_c were used as starting values and were individually fitted. The experiment only determines the absolute value of the TDM; the sign of the angle between the TDM vector and the a/b axes is undetermined, giving rise to two possible orientations, which are shown in Figure 6 as full-line and dashed-line black arrows. We prefer the full-line TDM orientation that lies closer to the TD-B3LYP calculated TDM (blue arrow). The latter lies close to the b inertial axis, with a ratio $|\mu_a|^2$:$|\mu_b|^2$ = 10:90. The contour fit yields $|\mu_a|^2$:$|\mu_b|^2$ = 26:74, implying that the experimental TDM is rotated by 25 toward the a axis; note that the experimental error is 9−10°.

Figure 7 compares the simulated (black) to the experimental (gray) contours of the 1_0^2, 2_0^2, and 3_0^2 overtone bands. To fit these contours, the parameters of the 0_0^0 band were taken as initial values. The A′ rotational constants and the A−A/E−E torsional subband splitting changed slightly and were refitted for each band, see Table 5.

D. Excited-State Lifetimes. The finite excited-state lifetime gives rise to a contribution to the bandwidth with a Lorentzian line shape, $\Delta_{Lor} = 1/2\pi\tau$. This was varied from Δ_{Lor} = 900 MHz, corresponding to a lifetime of τ = 180 ps, to 54 GHz, corresponding to τ = 3 ps. The effects of varying Δ_{Lor} for the 0_0^0 rotational contour are shown in Figure 8. We find the best agreement for Δ_{Lor} = 2700−5400 MHz, corresponding to τ = 30−60 ps, see Figure 8b,c. Given the laser resolution and the S/N ratio, we can clearly exclude that the lifetime of the vibrationless $^1\pi\pi^*$ state is less than 30 ps, as shown by the progressively poorer agreement with experiment in Figure 8d−f. On the other hand, the lifetime cannot be longer than τ = 180 ps, otherwise more discrete structure and a small central peak should be observed, see Figure 8a.

Δ_{Lor} was fitted for the 1_0^2 and 2_0^2 bands; the upper limit is also 2700 MHz (τ = 60 ps), as shown in Figure 7. The 3_0^2 contour clearly exhibits a deeper central dip and sharper structure than the other three bands. We have simulated the 3_0^2 contour with Δ_{Lor} = 900 MHz (τ = 180 ps). Although this is clearly the lower limit, we note that many of the expected features can be observed experimentally, as shown in Figure 7d. Table 5 summarizes the fitted parameters for all four bands.

E. Vibronic Band Assignments. We base the assignments of the vibronic bands on the CC2 and TD-B3LYP calculated $^1\pi\pi^*$ frequencies given in Table 4, which mutually agree within 15%. Note that the CC2 optimized S_2 minimum is more out-of plane than the B3LYP structure. Hence, the TD-B3LYP vibrations ν'_4 and ν'_6 are in-plane vibrations, but are out-of-plane when calculated with CC2. Below we refer to the TD-B3LYP frequencies. The assignments are summarized in Table 6. The most important out-of-plane normal-modes are illustrated in Figure 9 and the important in-plane normal-modes are shown in Figure 10.

dx.doi.org/10.1021/jp305688m | J. Phys. Chem. B 2012, 116, 11081−11091

Table 5. S_0 and S_2 ($^1\pi\pi^*$) State CC2/aug-cc-pVTZ and B3LYP/TZVP Calculated Rotational Constants of 5-Methylcytosine, E−A Torsional Subband Splitting Δ, Relative Transition Dipole Moment Components (in %), and Comparison to Fitted Values from Contour Simulations for the 0_0^0, 0_0^0 + 49, 0_0^0 + 69, and 0_0^0 + 167 cm^{-1} Bands[a]

parameters	CC2	B3LYP	0_0^0 band	1_0^2 band	2_0^2 band	3_0^2 band
A″ (MHz)	3151	3133				
B″ (MHz)	1413	1419				
B″ (MHz)	982	983				
A′−A″ (MHz)	−95	−55	−118 (80)	−200 (80)	−81 (80)	−220 (80)
B′−B″ (MHz)	−8	−1				
C′−C″ (MHz)	−13	−6				
Δ(E−A) (cm^{-1})		0.20	0.3(1)	0.2(1)	0.4(1)	0.2(1)
$\|\mu_a\|^2:\|\mu_b\|^2:\|\mu_c\|^2$ [a]		10:90:0	26(10):74(9):0(3)	(26:74:0)[c]	(26:74:0)[c]	(26:74:0)[c]
Δ_{Lor} (MHz)			2700	2700	2700	900
Δ_{Gauss} (MHz)			1555	1555	1555	1555
T_{rot} (K)			4.5 (1)	4.5 (1)	4.5 (1)	4.5 (1)

[a]Estimated uncertainties in parentheses. [b]Sum of transition dipole moment components normalized to 100%. [c]Value taken over from the 0_0^0 band.

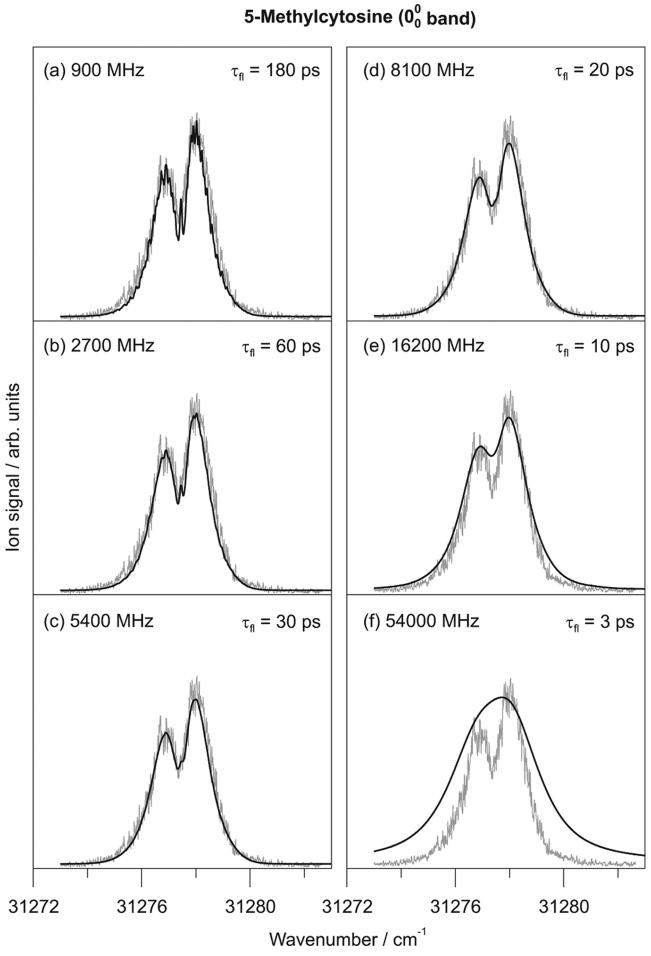

Figure 8. Simulations of the 0_0^0 band contour of 5-methylcytosine. The experimental contour (at 0.05 cm^{-1} resolution, ionization at 226 nm) is plotted in gray. The asymmetric rotor contours for an in-plane ($\pi\pi^*$) transition are superimposed in black, using six different excited-state lifetimes (τ_{fl} = 180 down to 3 ps). This results in Lorentzian line width contributions that range from (a) 900 to (f) 54 000 MHz. The other fit parameters are listed in Table 5.

Out-of-Plane Vibrations. The lowest-frequency mode ω_1 corresponds to the methyl group internal rotation relative to the rest of the molecule, which is poorly described in the harmonic approximation. Therefore, the levels, transitions and band intensities were calculated using a one-dimensional internal-rotation Hamiltonian as in refs 16 and 20. The internal rotation potentials were calculated at the B3LYP and TD-B3LYP levels and are shown in Figure 11. The barriers are rather high, $V''_3(S_0)$ = 851 cm^{-1} and $V'_3(S_2)$ = 197 cm^{-1}. This is due to the vicinity of the methyl and amino groups which hinders the rotation of the methyl group, see also Figure 2. The angles of the potential minima coincide in both electronic states. In combination with the high barriers, this leads to weak internal-rotation transitions that are typically <5% of the 0_0^0 band. The predicted positions and intensities are given in the Supporting Information. Indeed, no methyl rotor transitions could be observed in the R2PI spectrum, see below.

The $^1\pi\pi^*$ state out-of-plane deformation breaks the C_s symmetry in two symmetry-equivalent ways, leading to two equivalent nonplanar $^1\pi\pi^*$ minima. Thus, one expects out-of-

Table 6. Experimental $^1\pi\pi^*$ state band frequencies of 5-methylcytosine (in cm^{-1} relative to the 0_0^0 band) of 5-methylcytosine), measured by two-color R2PI spectroscopy, cf. Figures 4 and 5

assignment	rel. wavenumber
1_2^0	−194
1_2^2	−147
1_3^1	−80
1_2^3	−24
0_0^0	(31277.4)
$2\nu'_1$	48.5
$2\nu'_2$	69.2
$4\nu'_1$	109.5
$2\nu'_1+ 2\nu'_2$	127.2
$4\nu'_2$	143.4
$2\nu'_3$	166.8
$4\nu'_1+ 2\nu'_2$	183.4
$2\nu'_1+ 4\nu'_2$	194.1
$6\nu'_2$	216.9
$2\nu'_2+ 2\nu'_3$	234.1
$4\nu'_1+ 4\nu'_2$?	256.2
$4\nu'_2+2\nu'_3$	303.3
ν'_6	320.2
$\nu'_6+2\nu'_2$	385.7
$\nu'_6+4\nu'_2$	457.6
ν'_9	467.5
ν'_{10}	514.2
ν'_{17}	731.2

dx.doi.org/10.1021/jp305688m | J. Phys. Chem. B 2012, 116, 11081−11091

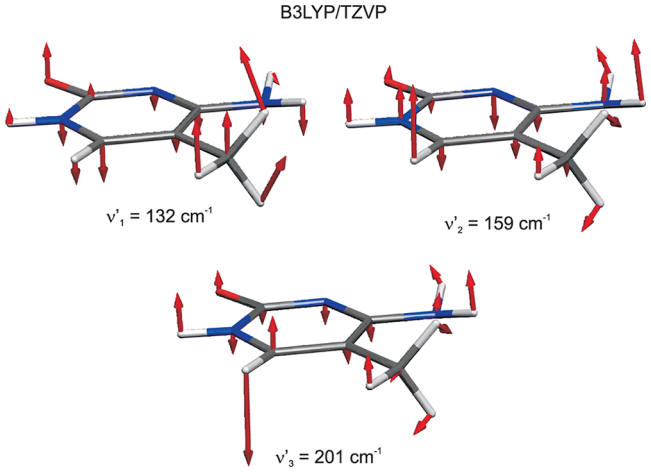

Figure 9. TD-B3LYP eigenvectors of the three lowest-frequency $\pi\pi^*(S_2)$ out-of-plane modes of 5-methylcytosine.

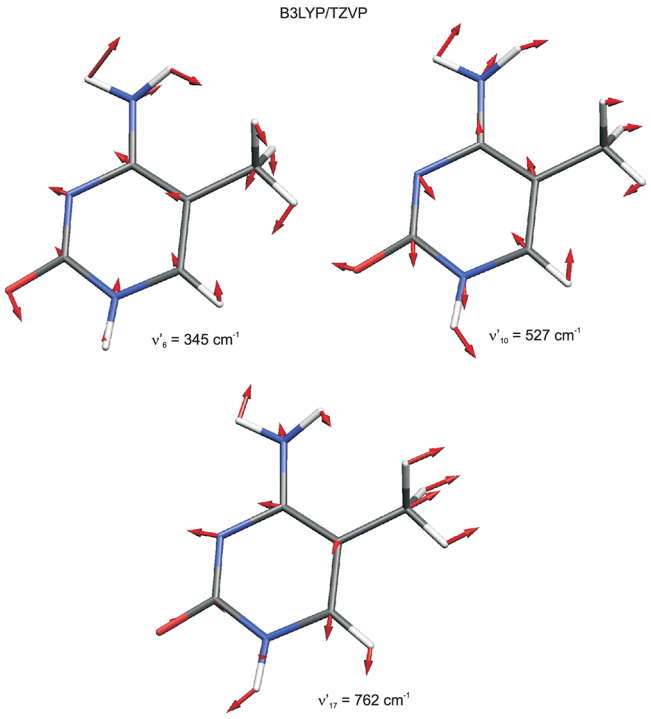

Figure 10. TD-B3LYP eigenvectors of the three optically active in-plane vibrations ν'_6, $\nu'_{10}(6a)$ and $\nu'_{17}(1)$ of 5-methylcytosine in the $\pi\pi^*(S_2)$ state.

plane (oop) vibrations to couple to the electronic excitation. The calculations predict that the low-frequency modes ν'_1, ν'_2, and ν'_3 are oop with low fundamental frequencies of 132, 159, and 201 cm^{-1}, respectively, see also Table 4. The calculated (oop) eigenvectors for ν'_1, ν'_2, and ν'_3 are shown in Figure 9.

The bands below 250 cm^{-1} lie lower than any of the calculated in-plane fundamental frequencies. Hence, they must be a′ overtones or combination bands of the oop vibrations. We assign the first intense band at 48.5 cm^{-1} as the overtone of the first oop mode, $2\nu'_1$, and the small band at 109.5 cm^{-1} to the $4\nu'_1$ overtone, see Table 6. Note the positive anharmonicity of this vibration, which implies a considerable quartic component in the potential.

The most intense band in the R2PI spectrum at +69.2 cm^{-1} is assigned to the overtone of the next oop vibration, $2\nu'_2$. This

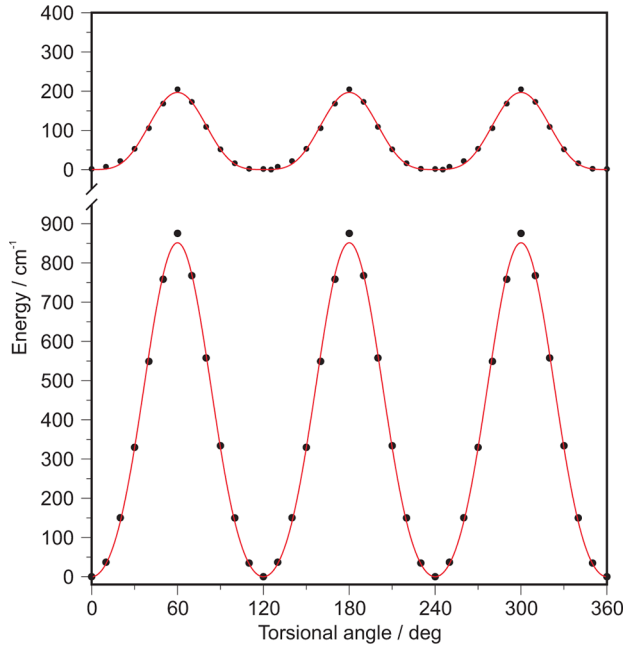

Figure 11. B3LYP and TD-B3LYP calculated S_0 and S_2 ($\pi\pi^*$) state methyl internal-rotation potentials for 5-methylcytosine (TZVP).

vibration exhibits an extended overtone progression with $4\nu'_2$ at 143.4 cm^{-1} and $6\nu'_2$ at 216.9 cm^{-1}. As for ν'_1, the anharmonicity is positive, albeit smaller. Given that the ν'_1 and ν'_2 vibrations exhibit prominent overtone bands, it is not surprising that several of their combinations appear strongly. We assign the bands at 127, 183, and 194 cm^{-1} to $2\nu'_1 + 2\nu'_2$, $4\nu'_1 + 2\nu'_2$, and $2\nu'_1 + 4\nu'_2$, respectively, see Table 6.

The lowest excitation that cannot be assigned as an overtone or a combination of ν'_1 and ν'_2 lies at 167 cm^{-1}. Because of its low frequency we assign it as the $2\nu'_3$ overtone. The calculations predict ν'_3 to be different from ν'_1 and ν'_2: When optimizing the $^1\pi\pi^*$ state to C_s symmetry, the normal-mode analyses yield an imaginary ν'_3 frequency, indicating a symmetric double-minimum potential along the Q'_3 coordinate. The TD-B3LYP barrier at the C_s geometry (corresponding to $Q'_3 = 0$) is 102 cm^{-1}. We fitted a quartic-plus-quadratic double minimum potential $V(Q'_3) = AQ'^4_3 + BQ'^2_3 + C$, which is shown in Figure 12, with parameters $A = 3.1$, $B = -36.05$, and $C = 102$ cm^{-1}. As constraints, we required the barrier height C to equal the calculated value (102 cm^{-1}) and the difference of the $\nu' = 0$ and 2 levels to agree with the experimental value 166.8 cm^{-1}, see Table 6. The third constraint was chosen by adjusting the vibrational reduced mass $\mu(Q'_3) = 0.1048$ so that with the locally harmonic potentials centered at $\pm Q_{3,min}$ the same fundamental frequency is obtained as with the TD-B3LYP harmonic calculation (200.6 cm^{-1}). The anharmonic eigenvalues for the lowest five vibrational states are shown in Figure 12. As for ν'_1 and ν'_2, vibronic excitations from the S_0 $\nu'' = 0$ state are only allowed to excited levels that are a′ in C_s. Beyond the 3^4_0 transition that was used to constrain the fit, the next predicted transition is 3^4_0 at 463 cm^{-1}; this is close to the break-off of the spectrum and cannot be clearly identified.

Many of the bands above 235 cm^{-1} in Figure 4 can be assigned as higher overtones or combinations of ν'_1, ν'_2, and ν'_3, as given in Table 6. However, there are additional weak bands in this region that are difficult to assign, indicating the

dx.doi.org/10.1021/jp305688m | J. Phys. Chem. B 2012, 116, 11081−11091

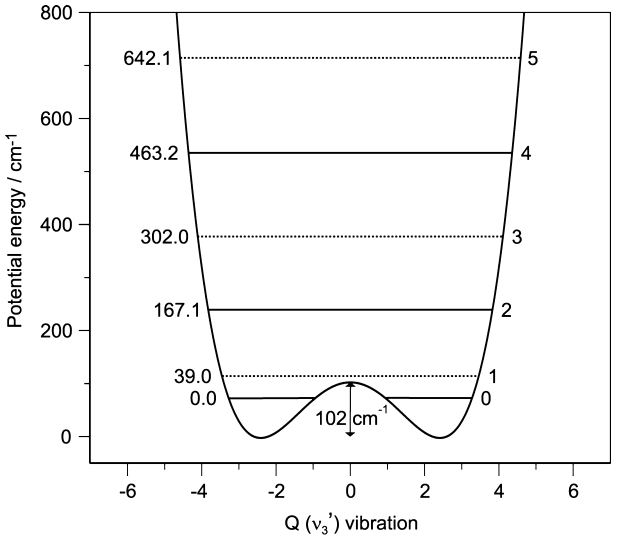

Figure 12. TD-B3LYP calculated $^1\pi\pi^*$ (S_2) state potential along the ν'_3 out-of-plane coordinate.

onset of strong anharmonicity around 250−500 cm^{-1} in the $^1\pi\pi^*$ state potential energy surface.

The amino inversion mode I exhibits double-minimum potentials in both states. Figure 13 shows the B3LYP and TD-B3LYP calculated NH_2 inversion potentials for S_0 and S_2. The S_0 potential has a tiny barrier of ~2 cm^{-1}. The S_2 state barrier is identical to that discussed for ν'_3 (102 cm^{-1}). The Boltzmann weighted FCFs of the I_1^1 and I_1^3 transitions are very small, since the ν'' = 1 (a″) ground state level, which is predicted at 347 cm^{-1}, is not populated. The I_0^2 inversion transition is predicted at ~670 cm^{-1} but cannot be observed experimentally, since the R2PI spectrum breaks off previously.

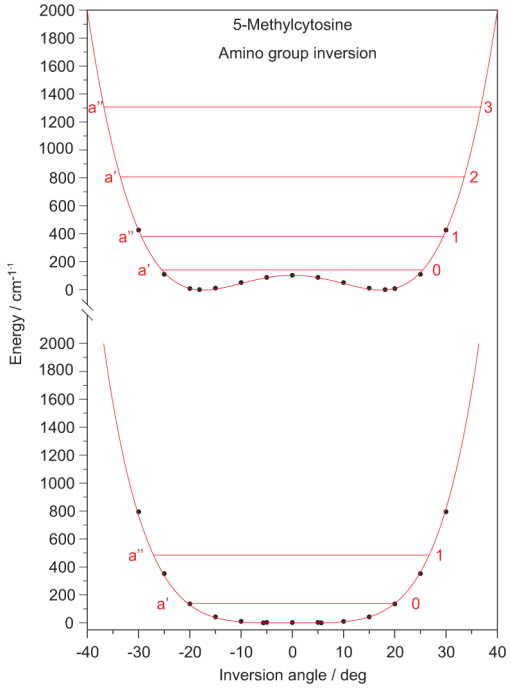

Figure 13. NH_2 inversion potential curve for 5-methylcytosine in the S_0 and $^1\pi\pi^*$ (S_2) states, calculated at the B3LYP and TD-B3LYP levels, and anharmonic energy levels (for details, see the text).

In-Plane Vibrations. The a′ in-plane fundamental vibrations are symmetry-allowed. Five in-plane vibrational fundamentals are predicted within 750 cm^{-1} above the 0_0^0 band, see Table 4. The lowest-energy band that we cannot assign to an out-of-plane combination or overtone is the medium intense excitation at 320 cm^{-1}, which we assign as ν'_6 (predicted at 326 cm^{-1}). This level then combines with the $2\nu'_2$ and $4\nu'_2$ overtones, giving rise to a three-membered progression.

The next band at 514 cm^{-1} is assigned as the in-plane ν'_{10} fundamental, predicted at 484 cm^{-1}. This mode is closely analogous to the 6a mode that appears strongly in the lowest $^1\pi\pi^*$ excitation of many benzene derivatives. The weak band at 731 cm^{-1} is assigned to ν'_{17}, predicted at 740 cm^{-1}. This vibration is analogous to the 1 vibration in benzene derivatives. The ν'_9 fundamental is predicted to lie at 469.6 cm^{-1}; it may possibly be assigned to the band at 467 cm^{-1}. The higher in-plane vibrations ν'_{12} (predicted at 539.9 cm^{-1}) and ν'_{16} (predicted at 719.4 cm^{-1}) are not observed in the spectrum.

IV. DISCUSSION

A. Out-of-Plane Vibronic Excitations. We have shown above that the first 12 vibronic bands of 5MCyt below ~300 cm^{-1} are excitations of overtones or combinations of the ν'_1, ν'_2, and ν'_3 out-of-plane vibrations. Based on their very low fundamental frequencies, we conclude that the excited-state potentials of 5MCyt along the Q'_1, Q'_2, and Q'_3 vibrational coordinates are extremely soft, with fundamentals $\nu'_1 \approx 24$ cm^{-1}, $\nu'_2 \approx 35$ cm^{-1}, and $\nu'_3 \approx 84$ cm^{-1} (estimated as half the first overtone frequency, see Table 4).

The out-of-plane fundamental harmonic frequencies calculated for the $^1\pi\pi^*$ state at the CC2 and TD-B3LYP levels massively overestimate the experimental values, i.e., by a factor of 4−5 for ν'_1 and ν'_2, and by ~2.5 for ν'_3. These large discrepancies for these vibrations are in line with previous experience with CIS and CAS-SCF excited-state vibrational calculations on 2-pyridone:[21] Although the in-plane vibrational frequencies are predicted quite accurately, the out-of-plane vibrational frequencies were found to be poor.[21] Although the large discrepancies between calculation and experiment for 5MCyt may also reflect shortcomings of the CC2 and TD-B3LYP methods, we believe that a major part of the difference originates from the large quartic components of the out-of-plane potential functions, as documented by the positive anharmonicities of ν'_1 and ν'_2 and the calculated potential energy function for ν'_3 (Figure 11). In such cases, the harmonic frequencies that the ab initio calculation determines from the local curvature of the potential at the nonplanar minima always strongly overestimate the true anharmonic frequencies.

The large Franck−Condon factors of the $2\nu'_1$, $2\nu'_2$, $4\nu'_2$, and $2\nu'_3$ overtones imply that the excited-state frequencies differ strongly from the ground state ones and/or that excited-state potential minima are substantially displaced from the ground-state C_s symmetric geometry. From the positive vibrational anharmonicities, it follows that the ν'_1 and ν'_2 vibrational potentials must be flat-bottomed with strong quartic components. As discussed above, the ν'_3 vibration exhibits a double-well potential with nonplanar minima that are strongly displaced from C_s-symmetric $Q'_3 = 0$ position, see Figure 12.

A vibronic band pattern resembling that of 5-methylcytosine with low-frequency intense 1_0^2 and 2_0^2 bands has been observed in the $S_1 \leftarrow S_0$ spectrum of 2-pyridone (2PY):[21] The vibronic band structure of 2PY also indicated excitation from a planar and C_s-symmetric S_0 state to a nonplanar $^1\pi\pi^*$ state. As with

dx.doi.org/10.1021/jp305688m | J. Phys. Chem. B 2012, 116, 11081−11091

5MCyt, the lowest out-of-plane frequency of 2PY is low, $\nu'_1 \approx 47$ cm^{-1}, and its potential along Q'_1 has a strong quartic component. The $2\nu'_2$ overtone of 2PY lies at 252 cm^{-1} and its potential along Q'_2 is double-minimum, analogous to Q'_3 for 5MCyt. The similarity of the frequencies and potentials of the low-frequency out-of-plane vibrations that couple to the lowest $^1\pi\pi^*$ excitations of 2PY and 5MCyt show that the nonplanarity of the two chromophores in the $^1\pi\pi^*$ state is intrinsic to ketopyridine and ketopyrimidine derivatives, and reflects the closely related π and π^* frontier orbitals of the two molecules. Significantly, the excited-state nonplanarity already appears upon introduction of the first keto-group into the pyridine framework.

B. Weak Bands to the Red of the Origin. The R2PI spectra exhibit several weak bands shifted by ~150 cm^{-1} below the 0^0_0 band of the amino-keto N_1H tautomer. Based on the holeburning spectrum, and in agreement with Nir et al.,[8] the possibility that these bands originate from the cold $\nu'' = 0$ level of the S_0 state can be definitely excluded. Weak $^1n_O\pi^*$ transitions are predicted 0.48 eV (CC2) or 0.18 eV (TD-B3LYP) below the $^1\pi\pi^*$ transitions, see Table 2. However, the holeburning spectrum also excludes that the weak bands belong to the $^1n_O\pi^*$ transition, because they would also start from the S_0 $\nu'' = 0$ level. While the bands would nicely fit the TD-B3LYP $^1\pi\pi^*$ adiabatic transition energy of the amino-keto N_3H (**4**) tautomer (see Table 2), the correlated methods all predict **4** to lie 7−8 kcal/mol above **1**, which implies a minute population of **4** in the supersonic jet. Alternatively, the weak bands might arise from fragmentation of the 5MCyt·H_2O cluster. However, we have not observed any ion signals in the 5MCyt·H_2O^+ mass channel. Also, the TD-B3LYP calculations predict the $^1\pi\pi^*$ adiabatic transition of 5MCyt·H_2O ~600 cm^{-1} to the blue of the 5MCyt **1** origin.

The only remaining interpretation is as hot bands of **1**, which agrees with the observation that the weak bands can be varied by changing the backing pressure, as can be seen by comparing Figures 4 and 5. The B3LYP and CC2 methods predicts the lowest-energy ground state vibration at $\nu''_1 = 89$ and 87 cm^{-1}, respectively; see also the Supporting Information. On the basis of these estimates, we propose a tentative assignment of four of the weak bands as the 1^1_1, 1^3_1, 1^1_2 and 1^0_2 excitations, see Table 6. This assignment implies that ν''_1 lies at 97 cm^{-1}, and that the upper-state odd levels lie at $\nu'_1 = 17$ cm^{-1} and $3\nu'_1 = 73$ cm^{-1}, but these values should be considered as very tentative.

C. Excited-State Lifetimes. Although no time-resolved experimental measurements have so far been performed on 5MCyt, two femtosecond pump−probe experiments of jet-cooled cytosine were performed at 267 nm (~37 450 cm^{-1}),[22,23] followed by a more detailed investigation by Kosma et al. at five wavelengths from 260−290 nm.[24] These show mono-, bi-, or triexponential decay profiles, depending on the time resolution and on the procedure employed to fit the decays.[22−24] The tautomer(s) of cytosine giving rise to the subps and ps decay times were not identified in the earlier work.[22,23] In the 280 and 290 nm measurements of Kosma et al., only the amino-keto N1H **1** tautomer can be excited, but at relatively high vibrational excess energies of 2700 and 3900 cm^{-1}, respectively.

In any case, the lifetime of 5-methylcytosine when excited at the 0^0_0, 1^2_0, 2^2_0, and 3^2_0 vibronic bands is $\tau = 30$−60 ps, or 20−60 times longer than the reported 1−1.5 ps[24] pump−probe lifetimes of keto-amino **1** cytosine. Although a part of the difference may be due to the 5-methylation, we propose that the much shorter fs pump−probe lifetimes reported for cytosine mainly reflect the different excited-state dynamics of the high vibrational states excited in the pump−probe experiments.[24]

V. CONCLUSIONS

We have measured the UV vibronic spectra of jet-cooled 5-methylcytosine (5MCyt) using two-color resonant two-photon ionization spectroscopy at 0.3 and 0.05 cm^{-1} resolution. In contrast to cytosine, whose lowest electronic transition shows only five vibronic bands above the origin, the spectrum of 5MCyt exhibits about 25 low-frequency bands. The majority of these are assigned to a′ overtone and combination levels of the three low-frequency out-of-plane vibrations ν'_1, ν'_2, and ν'_3. The appearance of intense out-of-plane overtones implies a loss of C_s symmetry and large geometry changes along the ring twisting (ν'_1), the butterfly (ν'_2), and the HN^1-C^6H twist (ν'_3) coordinates upon $^1\pi\pi^*$ excitation. The largest displacement is along ν'_2, which exhibits overtones up to $6\nu'_2$.

From the overtone frequencies the corresponding fundamentals are interpolated as $\nu'_1 = 24$, $\nu'_2 = 35$, and $\nu'_3 = 84$ cm^{-1}, respectively. These frequencies are between three to five times lower than the harmonic $^1\pi\pi^*$ state frequencies predicted by the CC2 and TD-B3LYP calculations. The poor agreement of theory with experimental values is due to the very flat or (for ν'_3) double-minimum potential energy curves; the strong anharmonicity limits the value of normal-mode calculations in such situations. This concurs with the observation of Marian and co-workers for cytosine that the $^1\pi\pi^*$ minimum is very flat.[18]

No methyl group internal-rotation bands are observed, in agreement with the predictions of the CC2 and B3LYP calculations that the methyl group orientation does not change upon $^1\pi\pi^*$ electronic excitation and the methyl rotor barriers are high in both the S_0 state ($V''_3 = 851$ cm^{-1}) and in the $^1\pi\pi^*$ state ($V'_3 = 197$ cm^{-1}).

The rotational contours of the first four intense bands (0^0_0, 1^2_0, 2^2_0, and 3^2_0) are a/b hybrids with no significant c-type contribution. For the 0^0_0 band, this implies that the electronic transition is polarized within the pyrimidinone plane and is $^1\pi\pi^*$. Furthermore, the 1^2_0, 2^2_0, and 3^2_0 overtone bands lead to a′ upper-state levels, which is consistent with the assignment. The experimental transition dipole moment ratio along the in-plane a/b axes is $|\mu_a|^2:|\mu_b|^2 = 25\%:75\%$ for all four bands, implying that the transition is polarized along the $N_1\cdots$amino direction, in good agreement with the TD-B3LYP calculated ratio for the $^1\pi\pi^*$ excitation. The absence of c-type contributions to these four bands implies that no significant $^1\pi\pi^* \leftrightarrow {}^1n\pi^*$ mixing occurs from the vibrationless S_1 level up to +170 cm^{-1} above.

To reproduce the widths and partial lack of fine structure of the rotational contours, significant Lorentzian linewidths had to be included into the simulations, reflecting the lifetimes τ of the $^1\pi\pi^*$ state levels $\nu'' = 0$, $2\nu'_1$, $2\nu'_2$, and $2\nu'_3$. Via the Lorentz contributions, we determined $\tau \geq 30$ ps for the four levels. The 3^2_0 band is significantly better resolved, its lifetime is certainly longer than 60 ps and might be up to $\tau = 180$ ps. These lifetimes are at least 30 times longer than the lifetime of the amino-keto **1** tautomer ($\tau = 1.1$−1.2 ps) determined by fs laser pump−probe spectroscopy.[24]

At vibrational energies ~250−350 cm^{-1} above the origin, the R2PI signal decreases rapidly and above +350 cm^{-1}, the widths of many bands increase up to 10 cm^{-1}. This implies that the

dx.doi.org/10.1021/jp305688m | J. Phys. Chem. B 2012, 116, 11081−11091

vibronic level lifetimes decrease to $\tau < 0.5$ ps or by a factor of 20 compared to excess energies <250 cm^{-1}. This suggests that the $^1\pi\pi^*$ state exhibits a barrier to radiationless relaxation that is located at about +350 cm^{-1}. We also note a sudden increase in the density of vibronic bands in the 250−350 cm^{-1} range, which indicates a flat part of the excited-state potential and provide a spectroscopic diagnosis of the approach to this barrier. Although there are no calculations for 5MCyt, for cytosine Marian and co-workers have predicted a barrierless (direct) approach to a conical intersection that is located 1600 cm^{-1} above the minimum of the $^1\pi\pi^*$ state.[18]

Following excitation in the low-frequency out-of-modes, the $^1\pi\pi^*$ state 5MCyt is carried through or over the barrier, followed by access to an efficient relaxation channel. Note that the spectrum exhibits intense overtone progressions of ν'_2 and that bands involving the $\nu'_6 + 2\nu'_2$ and $\nu'_6 + 4\nu_2'$ overtones are observed up to 458 cm^{-1}. This implies that the ν_2' butterfly vibration does not point directly toward the barrier. In contrast, the $4\nu'_1$ overtone at +105 cm^{-1} is abnormally weak compared to $2\nu'_1$. Similarly, the $2\nu'_3$ overtone, expected at ∼460 cm^{-1} is not observed. This implies that the "ring twisting" (ν'_1) and N1−C6H twist (ν'_3) vibrations efficiently propel the system toward the barrier, thereby promoting internal conversion to the S_0 state.

Excitations to the in-plane (a′) fundamental vibrations ν'_9, ν'_{10}, and ν'_{17} are observed at 468, 514, and 731 cm^{-1}, which is substantially above the breaking-off of the out-of-plane overtone structure in the R2PI spectrum. Obviously, the in-plane vibrational levels cannot directly access the part of the PES along the barrier to nonradiative relaxation, even though they lie energetically above it! We propose that the in-plane vibrations couple weakly to the manifold of out-of-plane vibrational overtones (and combination) levels, leading slow ($k \approx 10^{11}$ s^{-1}) IVR, which is then followed by internal conversion.

■ ASSOCIATED CONTENT

Ⓢ Supporting Information

Five tables with additional information as indicated in the text. This material is available free of charge via the Internet at http://pubs.acs.org.

■ AUTHOR INFORMATION

Corresponding Author

*E-mail: leutwyler@iac.unibe.ch.

Notes

The authors declare no competing financial interest.

■ ACKNOWLEDGMENTS

Financial support by the Schweiz. Nationalfonds (Project No. 200020-132540) is gratefully acknowledged.

■ REFERENCES

(1) Colot, V.; Rossignol, J.-L. *BioEssays* **1999**, *21*, 402−411.
(2) Suzuki, G.; Shiomi, M.; Morihana, S.; Yamamoto, M.; Mukai, Y. *Genes Genet. Syst.* **2010**, *85*, 377−382.
(3) Holliday, R.; Pugh, J. E. *Science* **1975**, *187*, 226−232.
(4) Riggs, A. D. *Cytogenet. Cell Genet.* **1975**, *14*, 9−25.
(5) Merchan, M.; Serrano-Andres, L. *J. Am. Chem. Soc.* **2003**, *125*, 8108−8109.
(6) Brauer, B.; Gerber, R. B.; Kabelač, M.; Hobza, P.; Bakker, J. M.; Riziq, A. G. A.; de Vries, M. S. *J. Phys. Chem. A* **2005**, *109*, 6974−6984.
(7) Serrano-Andrés, L.; Merchan, M. *J. Photochem. Photobiol. C* **2009**, *10*, 21−32.
(8) Nir, E.; Müller, M.; Grace, L. I.; de Vries, M. *Chem. Phys. Lett.* **2002**, *355*, 59−64.
(9) Nir, E.; Hünig, I.; Kleinermanns, K.; de Vries, M. S. *Phys. Chem. Chem. Phys.* **2003**, *5*, 4780−4785.
(10) Bakker, J. M.; Compagnon, I.; Meijer, G.; v. Helden, G.; Kabelač, M.; Hobza, P.; de Vries, M. S. *Phys. Chem. Chem. Phys.* **2004**, *6*, 2810−2815.
(11) Lapinski, L.; Nowak, M. J.; Fulara, J. *J. Phys. Chem.* **1990**, *94*, 6555−6564.
(12) Feyer, V.; Plekan, O.; Kivimäki, A.; Prince, K. C.; Moskovskaya, T. E.; Zaytseva, I. L.; Soshnikov, D. Y.; Trofimov, A. B. *J. Phys. Chem. A* **2011**, *115*, 7722−7733.
(13) TURBOMOLE *V6.0 2009*; a development of Universität Karlsruhe (TH) and Forschungszentrum Karlsruhe GmbH, 1989−2007, TURBOMOLE GmbH, since 2007; available from http://www.turbomole.com.
(14) Tian, S. X.; Xu, K. Z. *Int. J. Quantum Chem.* **2002**, *89*, 106−120.
(15) Varsanyi, G. *Assignments for Vibrational Spectra of 700 Benzene Derivatives*; ADAM HILGER LTD: London, 1974.
(16) Lobsiger, S.; Frey, H. M.; Leutwyler, S.; Morgan, P.; Pratt, D. *J. Phys. Chem. A* **2011**, *115*, 13281−13290.
(17) Lobsiger, S.; Sinha, R. K.; Trachsel, M.; Leutwyler, S. *J. Chem. Phys.* **2011**, *134*, 114307−114320.
(18) Tomic, K.; Tatchen, J.; Marian, C. M. *J. Phys. Chem. A* **2005**, *109*, 8410−8418.
(19) PGOPHER 6.0.111, *C. M. Western*; a Program for Simulating Rotational Structures; available from http://pgophr.chm.bris.ac.uk.
(20) Lobsiger, S.; Frey, H. M.; Leutwyler, S. *Phys. Chem. Chem. Phys.* **2010**, *12*, 5032−5040.
(21) Frey, J. A.; Leist, R.; Tanner, C.; Frey, H.-M.; Leutwyler, S. *J. Chem. Phys.* **2006**, *125*, 114308−114321.
(22) Kang, H.; Lee, K. T.; Jung, B.; Ko, Y. J.; Kim, S. K. *J. Am. Chem. Soc.* **2002**, *124*, 12958−12959.
(23) Canuel, C.; Mons, M.; Piuzzi, F.; Tardivel, B.; Dimicoli, I.; Elhanine, M. *J. Chem. Phys.* **2005**, *122*, 74316−74321.
(24) Gonzalez-Vazquez, J.; Gonzalez, L.; Samoylova, E.; Schultz, T. *Phys. Chem. Chem. Phys.* **2009**, *11*, 3927−3934.
(25) Fogarasi, G. *J. Mol. Struct.* **1997**, *413*, 271−278.